Fuel 203 (2017) 68–81

Contents lists available at ScienceDirect

Fuel

journal homepage: www.elsevier.com/locate/fuel

Full Length Article

Effect of the properties of Silurian shales from the Barrandian Basin on their methane sorption potential

Zuzana Weishauptová *, Oldřich Přibyl, Ivana Sýkorová, Miloš René

Institute of Rock Structure and Mechanics, Academy of Sciences of the Czech Republic, 182 09 Prague 8, Czech Republic

HIGHLIGHTS

- High-pressure methane isotherms were measured on Czech Silurian shale samples.
- Maximum measured excess sorption and Langmuir sorption capacity were used.
- The methane excess sorption shows a positive correlation with TOC and clay contents.
- The highest sorption capacity was in shales with the lowest volume of micropores.
- No correlation was observed between maturity and methane sorption capacity.

ARTICLE INFO

Article history:
Received 24 November 2016
Received in revised form 13 April 2017
Accepted 19 April 2017
Available online 27 April 2017

Keywords:
Methane sorption capacity
Silurian shales
Barrandian Basin
Thermal maturity
TOC
Clays
Porous structure

ABSTRACT

High-pressure methane sorption isotherms were measured on seven representative samples of Silurian shales from the Barrandian Basin, Czech Republic. Excess sorption measurements were performed at a temperature of 45 °C and at pressures up to 15 MPa on dry samples, using a manometric method. Experimental methane high-pressure isotherms were fitted to a modified Langmuir equation. The maximum measured excess sorption parameter (n_{max}) and the Langmuir sorption capacity parameter (n_L) were used to study the effect of TOC content, organic maturity, inorganic components and pore size distribution on the methane sorption capacity. The values of n_{max} ranged from 0.050 to 0.088 mmol.g^{-1}, and the values of n_L ranged from 0.068 to 0.133 mmol.g^{-1}. The studied shale samples with random reflectance R_r of graptolite 0.56–1.76% had a very low TOC content from 0.34 to 2.37 wt% and dominant mineral fractions. Illite was the prevailing clay mineral (0–51%). Organic matter of the Silurian black shales was consisted of residues of graptolites, chitinozoans, two types of bitumen including dispersed and massive bitumens, recycled organic matter, and organic detritus. In the shales, the occurrence of fractures parallel with the original sedimentary bending was highly significant. A greater proportion of fragments of carbonaceous particles of graptolites and bitumens in the Barrandian shales had a smooth surface without pores. The sample porosity Por_{calc} ranged from 4.6 to 18.8%. In most samples, the micropore volumes were markedly lower than the meso- and macropore volumes. No relation has been proven between TOC-normalized excess sorption capacities or the TOC-normalized Langmuir sorption capacities and thermal maturation of the shales. The methane sorption capacities of shale samples show a positive correlation with TOC and a positive correlation with the clay content. The assumption that the sorption capacity is a function mainly of the microporous system of shales was not confirmed. The highest sorption capacity was observed in shale samples with the lowest volume of micropores and the highest TOC content, indicating that the organic matter content and the microporosity of clay minerals are the principal factors affecting the sorption capacity of shale samples.

1. Introduction

Although shale gas-bearing deposits have a markedly lower gas content than coal deposits, great attention has recently been paid to shale gas as a new potential source of fossil energy. Shale gas extraction is considered to be quite economical, despite the lower sorption capacity of shales, which is only about 10% of coal sorp-

* Corresponding author.
E-mail address: weishauptova@irsm.cas.cz (Z. Weishauptová).

http://dx.doi.org/10.1016/j.fuel.2017.04.087
0016-2361/

tion capacities [1]. A common feature of these unconventional sources of energetic gases – coalbed methane and shale gas – is a porous system bearing the collector properties. On the basis of present-day experience, it has been suggested that shale gas consists of a "free" gas, compressed in pores and fissures with no interaction with the shale matter, together with gas sorbed in the organic and mineral components of the rock, and gas dissolved in the deposit liquids [2,3]. The sorbed gas, which is crucial for the long-term stable production of shale gas [4], includes gas adsorbed in micropores, gas adsorbed on the surface of meso-, macro- and coarse pores, and gas dissolved (absorbed) in the macromolecular structure of kerogen and bitumen [5,6]. The sorption capacity is determined in the laboratory by measuring the amount of methane absorbed in a shale specimen at a pressure and a temperature corresponding to *in situ* conditions, using high pressure sorption. According to the principles of reversibility of adsorption/desorption, this amount should be roughly related to the amount of gas released by forced degassing.

The capacity of the porous system of shale is closely connected with its composition, i.e., with the abundance of organic (bitumen and zooclasts) and inorganic matter in a heterogeneous mixture. The organic matter is considered to be a major source of gas, which originated from thermogenic or biogenic processes. The amount of deposited gas is connected with the type and the abundance of organic matter, its degree of maturation, and its porosity. Porous clay minerals as a part of the inorganic fraction are not a source of gas, but through their sorption properties they are an important factor affecting the sorption capacity of the shale [7,8]. The total sorption capacity corresponds to the combined effect of the porosity of the organic matter and the clay minerals. Shale samples with a strong effect of total organic carbon (TOC) usually have a low concentration of clay minerals, and shale samples with a weak effect of TOC usually have a high concentration of clay mineral [2,9]. According to numerous studies, the contribution of clay minerals to the total sorption capacity is quite significant in dry shale samples with low TOC [3,10–12].

Shales have a very complex system of pores of various types and with a wide range of size classes. However, as far as sorption ability is concerned, micropores with diameters < 2 nm are generally considered to be the most important class. They have higher sorption energy than large pores [13], and therefore have a dominant effect on the shale sorption capacity. This has been confirmed by numerous studies [9,10,14,15]. Shale samples with high degrees of maturation and with high TOC levels have high sorption capacity. This can be explained by the formation of more micropores in the process of organic matter degradation and hydrocarbon formation with increasing thermal maturation [10]. Chalmers and Bustin concluded that the TOC content is the primary factor affecting the sorption capacity, and that the type of organic matter and its maturation can be considered as secondary factors [14].

The sorption capacity of clay minerals and clay-rich rocks has also been studied. It was found that the sorption affinity of methane is markedly stronger for organic matter than for clay minerals [4,12], though Ross and Bustin [10] determined that the sorption capacity of illite and montmorillonite was comparable with the sorption capacity of shales with high TOC levels. Some authors have found positive correlations between content of clay minerals and sorption capacity [3,12], while other authors have not observed a correlation of this kind [11,16].

Most published studies on the sorption capacity of shales deal with North American shales [17]. Extensive research has also been presented on Chinese shales [2,16,18–20]. Sorption experiments on European shales have only recently been reported [1,3,11,21–23]. The Czech Republic has been characterized only marginally for the potential of its shale gas deposits. The Prague Basin (Barrandian) is a locality where, according to the Czech Geological Survey, the presence of gas-bearing shales can be expected.

The present study has set out to determine the sorption capacities of selected shale samples from the Barrandian Basin, and to find connections with their petrographic, textural and mineralogical properties. The data obtained for the shales should also contribute to the European database.

2. Experimental

2.1. Samples

Representative samples of dark Silurian shales were taken from five quarries and outcrops located in the central part of the Barrandian basin (Fig. 1) from the basic Silurian lithostratigraphic formation (Fig. 2). [24,25]. Two samples were collected from the Litohlavy formation (S1 and S2), four samples from the Motol formation (S3, S5, S6 and S7), and one sample from the Kopanina formation (S4). The samples were collected after removing an approximately 50 cm upper layer of the outcrop. The basic geochemical properties are presented in Table 1.

2.2. Experimental methods

2.2.1. Petrographic analysis of dispersed organic matter

The reflectance of dispersed organic matter was measured on polished X-Y sections of rocks slabs, i. e. perpendicular to the banding or the foliation of the rocks studied here. Due to the absence of vitrinite in the Silurian Barrandian shale, the samples were measured for random reflectance (R_r%) of graptolite in normal light at λ = 546 nm, using a Carl Zeiss Axio Imager M2m microscope with a spectrometer with oil lenses (magnification of 50× and 100×). Yttrium-aluminium-garnet (R = 0.900%), gadolinium-gallium-garnet (R = 1.717%), cubic zirconia (R = 3.06%), and strontium-titanate (R = 5.34%) reflectance standards were used for calibrating the measurements. The composition of the organic particles differentiated by morphology and by optical properties into groups of graptolites, chitinozoans, bitumens, recycled organic matter and organic detritus [26–30], was determined using an Olympus BX51 microscope in normal light and fluorescence mode and with dry and oil lenses (magnification 40× and 100×) and a Pelcon point counter according to the principles of maceral analysis described in ISO 7404-3 [31]. The graptolite group contains lath-shaped fragments, a section of cortical tissues, and occasional remnants of thecae 10–300 μm in size. They were composed of a chitinous substance or a collagen-like protein that exhibited optical properties in reflected light similar to the properties of vitrinite. Chitinozoans occur as single microfossils or as chains of microfossils. They are flask- shaped or bottle-shaped, 50–250 μm in length, and they consist of an oral tube and a chamber with appendices. Massive (non-granular) and granular solid bitumen accumulates in intergranular pore spaces and microfractures. Non-granular bitumen can be observed in shales as rounded, oval or irregular bodies, while granular bitumen has an irregular formation and is also abundant as matrix bitumen. Highly reflecting fragments of zooclasts, bitumens, and other organic types of apparently allochtonous nature were classified as recycled organic matter. The last type of organic matter was organic detritus of unknown origin with particles below 10 μm in size.

2.2.2. TOC and mineralogical analysis

The elemental organic composition was determined using a CHNS/O micro-analyzer (Thermo Finnigan Flash FA 1112). TOC was determined by elemental analysis after inorganic carbonates had been eliminated with the use of 1 N HCl heated to 80 °C.

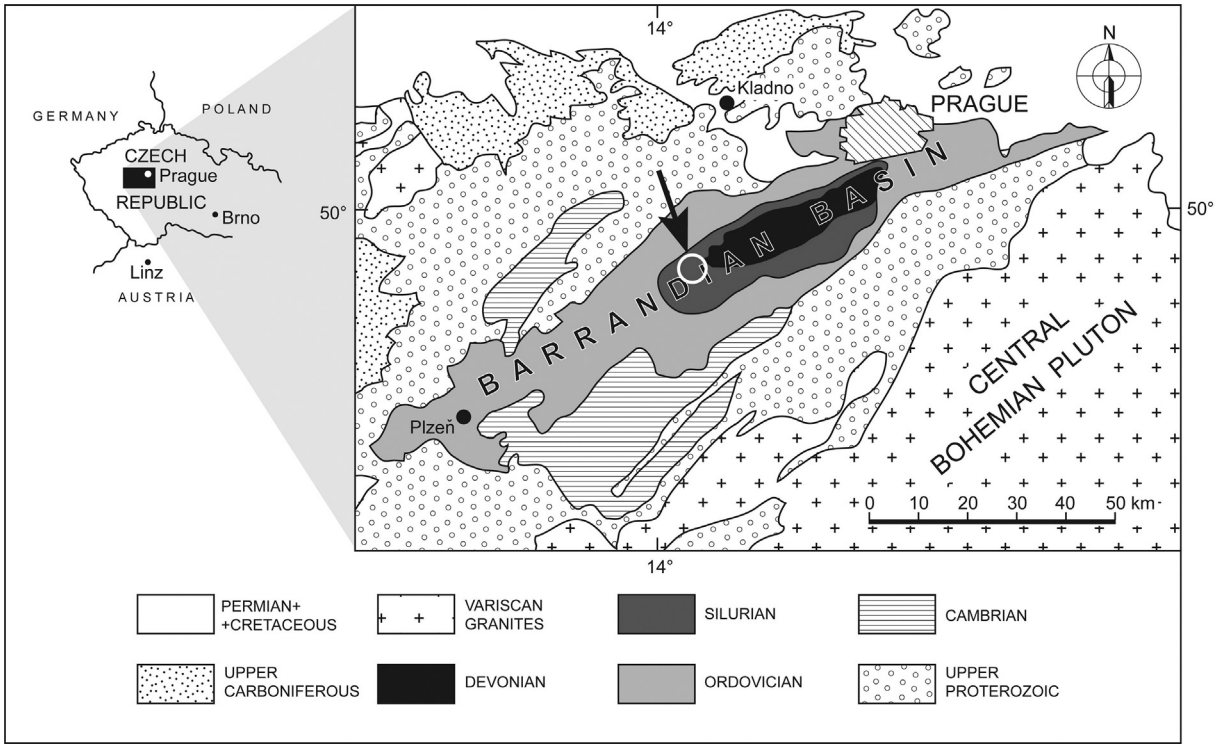

Fig. 1. Simplified geological map of the Barrandian Basin. Position of the outcrops from which the seven samples were taken.

The mineralogical composition of the shales was determined using X-ray diffraction (XRD) analyses. The size fraction of clay minerals at levels below 4 μm was prepared by the conventional sedimentation method. Randomly-oriented samples and settled air-dried samples (untreated, ethylene glycol solvated and heated to a high temperature (500 °C)) were analyzed using a Bruker D8 Discover diffractometer with CuKα radiation (40 kV, 40 mA), an Ni filter standard set and a scanning speed of 1°.min^{-1}.

Electron microprobe (SEM) analyses of selected minerals (feldspars, clay minerals, carbonates, sulfites) were carried out using a CAMECA SX 100 electron microprobe working in WDX mode employing the PAP matrix correction program [32]. The operating conditions for the analyses of the silicates and carbonates were 15 kV acceleration voltage, 15 nA beam current, and 2 μm beam diameter. The operating conditions for the analyses of the sulfites were 25 kV acceleration voltage and 20 nA beam current. The counting times on the peaks were 10–30 s, depending on the element. The background counts were measured in each case in half the time for peak measurements on both sides of the peak. Calibrations were made using reference materials from SPI.

2.2.3. Microscopic pore structure study

An FEI Quanta 450 scanning electron microscope with GAD detector was used to observe the microstructure morphology. It was able to produce images of the pore structure and the fracture morphology with resolution of 4.0 nm.

2.2.4. Mercury intrusion porosimetry

The volume of meso- (V_{meso}) and macropores (V_{macro}), their pore size distribution, average pore radius (r_{avrg}), surface area of meso- and macropores (S_{mm}), and bulk density (ρ_{bulk}) [33] were determined with particles 3–4 mm in size, using a Pascal 240 porosimeter by Thermo Electron – Porotec. The Pascal 240 porosimeter works within the 0.1–200 MPa pressure range, where pores with equivalent radii ranging from 3.7 nm to 7.5 μm can be detected. The samples were evacuated at 80 °C for 2 h prior to analysis, and were then evacuated in the instrument until stable pressure was reached. The results represent the average value from two measurements.

2.2.5. Low-pressure N_2 and CO_2 physisorption

Specific surface areas (S_{BET}) were determined from the N_2 isotherms measured at −196 °C, using the BET method in the 0.05–0.3 relative pressure range [34]. A Surfer (Thermo Scientific) volumetric sorption analyser was used.

The parameters characterizing the microporous texture, i.e., the total micropore volume (V_{micro}), the modus of the micropore radii (r_{mode}), and the micropore distribution were determined from the CO_2 sorption isotherm measured at a temperature of 25 °C up to a relative pressure of 0.015, using a Hiden IGA 100 gravimetric sorption analyzer. The micropore volume was calculated according to the Dubinin equation of volume filling [35], and the pore distribution was evaluated according to Medek [36]. Before the measurements, the samples with grain size < 0.2 mm were degassed in the instruments at a temperature of 80 °C under vacuum 10^{-6} Pa for at least 6 h up to a constant weight. The real helium density of the dry samples was determined using a Multipycnometer Quantachrome apparatus.

2.2.6. High pressure CH_4 sorption

The theoretical principles of the manometric method for measuring the high pressure sorption isotherm described in Ref. [37] are based on pressure changes in the system caused by the sorption process. The high pressure sorption isotherms of methane were measured using a manometric sorption apparatus in the arrangement depicted schematically in Ref. [37]. The main parts of the apparatus are a calibrated stainless-steel sample cell and a reference cell, automatically controlled valves and pressure transducers. The measuring pressure within the entire pressure range has accuracy of 0.05%, and the apparatus can be utilized within

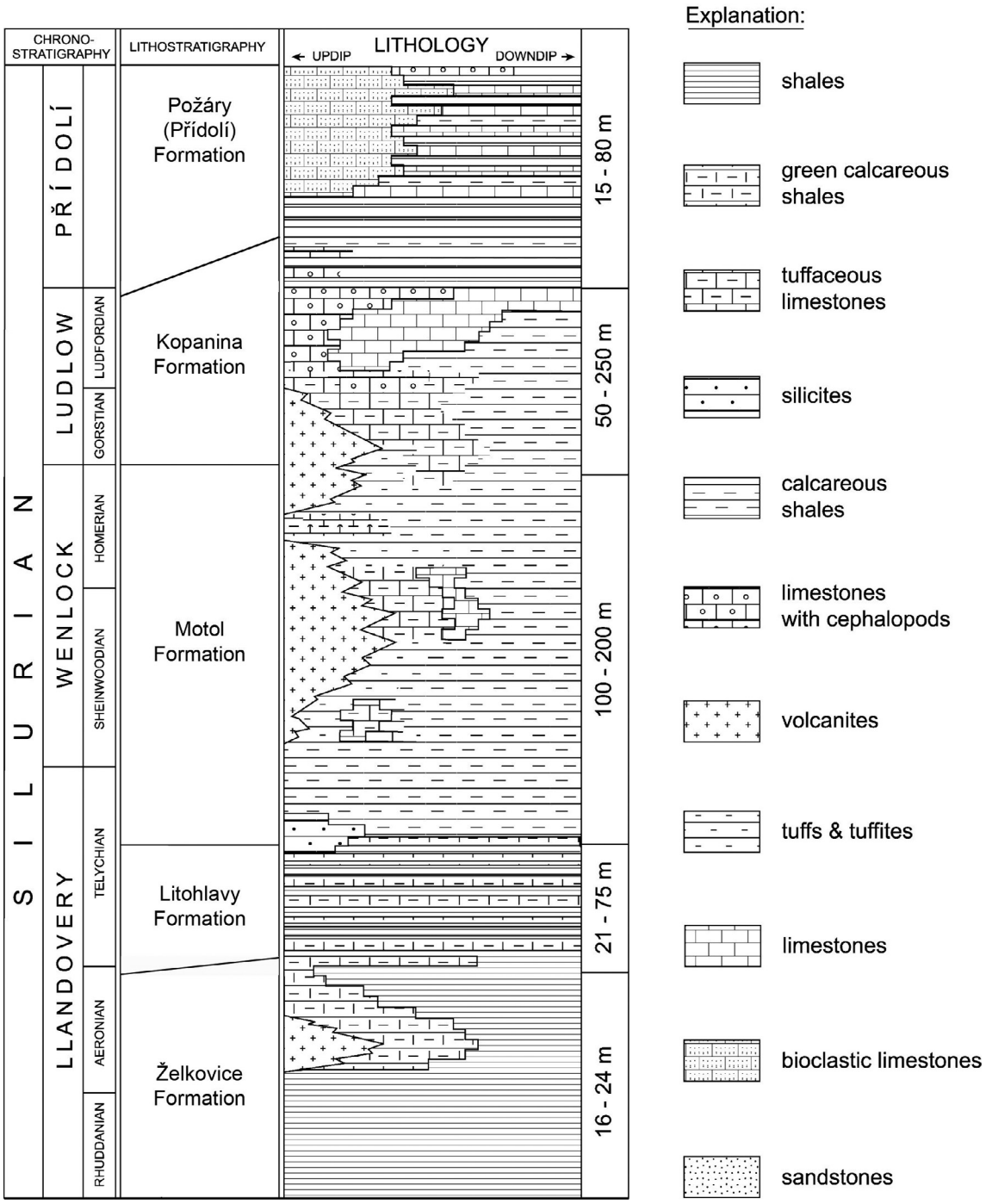

Fig. 2. Silurian lithostratigraphy and facies development of the Barrandian Basin according Kříž et al. [25].

the temperature range from 25 to 80 °C. The sorption device is placed in a thermostatic box, which is able to maintain a constant temperature within the range from 25 to 200 °C with accuracy of ±0.1 °C. The temperature of the sorption cell is controlled by an Ni–Cd thermocouple. The apparatus is controlled by a computer code created in the environment of the Control Web system, which also records and processes the measured data.

The volumes of the sample cell (V_s) (11.23 ± 0.01 cm^3) and the reference cell (V_r) (2.166 ± 0.002 cm^3) were determined by helium expansion, using steel cylinders of known dimensions which were placed into the sorption cell. The void volume (V_0) was defined by helium expansion, and was calculated as the average value from about 10 pressure steps in the range from 1 to 10 MPa with standard deviation less than 0.06%. The void volume was determined in order to calculate the skeletal density of the sample (ρ_{sample}). Before each sorption experiment, the equipment was tested for leakage by helium at 12 MPa for 4 h. The high pressure CH_4 excess sorption isotherms were measured on dry shale samples weighing approximately 9.5 g with grain size in the range of 0.2–0.05 mm at a temperature of 45 °C and at pressures up to 15 MPa. The shale samples were crushed with minimum fines to less than 0.05 mm. Before the measurements were made, the samples were dried at 80 °C under vacuum overnight and subsequently for approximately 4 h in a sample cell at 75 °C and vacuum. Methane

Table 1
Basic characterization of studied shale samples.

Sample	Formation	Parameter						
		R_r	A^d	C^d	TOC	S_t^d	S_{so4}^d	S_p^d
		(%)	(wt%)					
S1	Litohlavy	1.09	86.97	3.63	0.34	0.32	0.26	0.05
S2	Litohlavy	1.04	85.53	3.91	1.19	0.17	0.15	0.02
S3	Motol	0.89	87.32	4.23	2.37	1.07	0.01	0.98
S4	Kopanina	0.56	94.32	1.00	0.63	0.26	0.07	0.18
S5	Motol	0.94	88.73	3.88	2.33	1.15	0.01	1.11
S6	Motol	1.76	95.11	1.60	1.50	0.13	0.02	0.11
S7	Motol	0.93	70.71	7.97	0.43	0.08	0.00	0.08

R_r – random reflectance of graptolite, A – ash, C – carbon, S_t – total sulfur content, S_{so4} – sulfate sulfur, S_p – pyritic sulfur, d – dry basis.

sorption equilibrium on the shale samples was reached after about 3 h.

2.2.7. Parametrization of the experimental sorption isotherm

Experimental CH_4 high pressure isotherms were fitted to the modified Langmuir equation for monomolecular sorption [38]:

$$n_{ads} = n_L \cdot \frac{p}{p_L + p}\left(1 - \frac{\rho_{free}}{\rho_{ads}}\right), \quad (1)$$

where n_L is Langmuir sorption capacity, p_L is Langmuir pressure, ρ_{ads} is the density of the adsorbed phase, and ρ_{free} is the density of the free (gas) phase.

The value of ρ_{ads} (CH_4) = 0.420 g.cm^{-3} was utilized by solving Eq. (1) [39]. An equation by Setzmann and Wagner [40] was used for determining the free phase density $\rho_{free}(CH_4)$ under the experimental conditions. The accuracy of the approximation was expressed by parameter Δn, calculated by the equation:

$$\Delta n = \frac{1}{N}\sqrt{\sum_{1}^{N}(n - n_{fit})^2}, \quad (2)$$

where N is the number of data points of the isotherm, and n and n_{fit} are the measured and calculated sorbed amounts at points n.

3. Results

3.1. CH_4 sorption capacity of shale samples

Fig. 3 presents the high pressure excess sorption isotherms of CH_4 determined in shale samples S1–S7 at a temperature of 45 °C and at pressures up to 15 MPa, along with the curves fitted using the modified Langmuir equation (Eq. (1)). In all shale samples, the CH_4 high pressure excess sorption isotherm data at a temperature of 45 °C shows a sharp slope up to a pressure of 3 MPa, followed by a slight increase. At pressures exceeding 9–10 MPa, the isotherms show a slight decrease in sorption, with the exception of shale sample isotherms S3 and S5. The parametrization of the experimental sorption isotherms using the modified Langmuir equation, which is the most frequently-applied equation for describing high pressure sorption, shows a low deviation between the measured and fitted values (2.10^{-4}–7.10^{-4} mmol.g^{-1}). The graphs in Fig. 3 show that the quality of the fits is good. The shale samples with the highest maximum measured excess sorption (n_{max}) have the lowest approximation accuracy (Table 2). Table 2 presents the measured values of the maximum excess sorption (n_{max}), the pressure at maximum sorption ($p(n_{max})$) and the parametrization values, i.e. Langmuir sorption capacity (n_L) and Langmuir pressure (p_L). It shows that the sorption values range from 0.050 mmol.g^{-1} to 0.088 mmol.g^{-1} for n_{max}, and from 0.068 mmol.g^{-1} to 0.133 mmol.g^{-1} for n_L. This is approximately consistent with results presented by other authors [2,10].

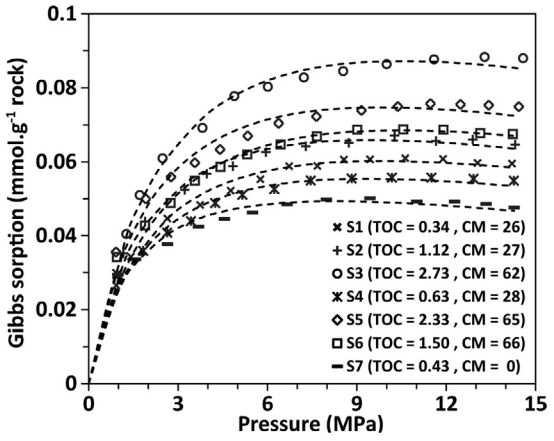

Fig. 3. CH_4 excess sorption isotherms on dry shale samples. The fit has been calculated using Langmuir Eq. (3), (TOC (wt%) – total organic carbon, CM (wt%) – clay minerals).

3.2. Shale composition

3.2.1. Organic maturity and organic components

The shales are uniformly dark grey and black. They are fissile, and they locally exhibit millimeter-scale fine lamination, particularly sample S7 (Fig. 4). The rock fractures are even, in most cases revealing clean fracture edges. The exceptions are samples S1 and S6; where rugged fractures frequently show up. The black shales of the Barrandian Basin studied here contain specific assemblages of organic matter (Fig. 5) that consist primarily of residues of graptolites, chitinozoans, two types of bitumen including dispersed and massive bitumens, recycled organic matter, and organic detritus. Fig. 5 shows a predominance of graptolites in samples S1, S2, S4, S6 and S7, while in samples S3 and S5 is more of both forms of bitumen. There was less occurrence of chitinozoans than graptolites, up to 15 vol% in samples S4 and S6.

The most common zooclast remains in the studied sediments were non-granular, optically isotropic graptolites and graptolite fragments (Fig. 6A and B). Their random reflectance R_r values ranged from 0.56% to 1.76%, see Table 1. This corresponds to a vitrinite reflectance equivalent 0.51–1.62% R_r when was found using Cole's conversion [41] and Gentzis's et al. [42] modification. In this study, based on Suchý et al. [43], the random reflectance values of graptolite (R_r) instead the vitrinite reflectance equivalent were used to determine the thermal maturity of the Silurian sediments in the Barrandian Basin. Random reflectance values of optically isotropic chitinozoan particles (Fig. 6C) ranged from 0.59% in a sample from the Kopanina formation to 1.10% in a sample from the Litohlavy formation and 1.74% in a sample from the Motol formation.

Table 2
Results of high-pressure CH_4 sorption on shale samples.

Sample	Experimental			Langmuir eq.		
	ρ_{sample} (g.cm^{-3})	n_{max} (mmol.g^{-1})	$p(n_{max})$ (MPa)	n_L (mmol.g^{-1})	p_L (MPa)	Δn (mmol.g^{-1})
S1	2.69	0.061	10.62	0.090	2.46	4.10^{-4}
S2	2.65	0.066	10.26	0.099	2.26	4.10^{-4}
S3	2.59	0.088	11.59	0.133	2.92	7.10^{-4}
S4	2.64	0.056	11.50	0.080	2.18	5.10^{-4}
S5	2.65	0.075	11.46	0.111	2.45	7.10^{-4}
S6	2.63	0.069	10.55	0.105	2.87	2.10^{-4}
S7	2.74	0.050	10.01	0.068	1.63	5.10^{-4}

ρ_{sample} – sample density (according to V_0), n_{max} – maximum measured excess sorption, $p(n_{max})$ – pressure at maximum sorption, n_L – Langmuir sorption capacity, p_L–Langmuir pressure, Δn – approximation accuracy.

Fig. 4. Detail of representative sample of dark brown, finely laminated calcareous shale (Motol formation, sample 7). The scale bar is 30 mm.

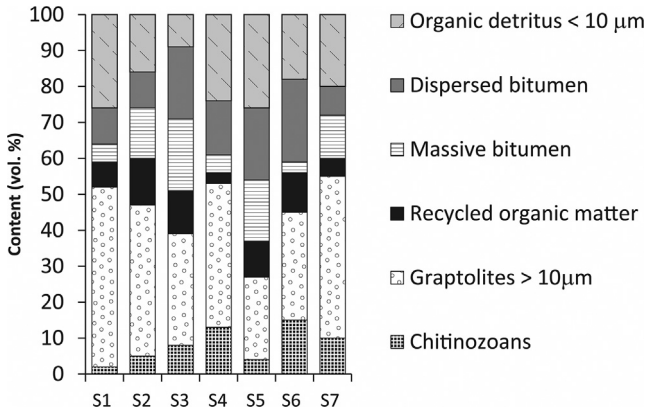

Fig. 5. The distribution of dispersed organic matter types in shale samples.

The reflectance values of non-granular bitumen bodies with internal pores, fissures and frequent surface inhomogenities (Fig. 6D) range from 0.50% to 1.10% and in sample S6 up to 1.85%. Reflectance values of granular bitumen range between 0.25% and 0.50%, and weak yellow-orange fluorescence was observed in all samples, with exception of sample S6. High reflecting bitumen without fluorescence color was found in sample S6. The highest reflectance values between 1.30% and 5.42%, were measured in recycled organic particles (Fig. 6C).

3.2.2. Inorganic components

The mineral composition of the shales, obtained from XRD analysis, is shown in Table 3. The analysed shales are fine-grained rocks which display some variation in their mineralogical composition and consist of quartz (10–30 wt%), calcite (0–76 wt%), illite (0–51 wt%), plagioclase (0–21 wt%) and chlorite (0–38 wt%). The dominant clay mineral is illite. K-feldspar, pyrite, sphalerite, apatite and zircon are accessories. Minute amounts of gypsum occurred as a secondary mineral originating from later oxidation of pyrite. Plagioclase is albite, but andesine was also found. Pyrite occurs as framboidal grains up to 0.1 mm in size, and/or as thin vein-like accumulations and veins. The occurrence of pyrite corresponds with the content of pyritic sulfur, which is presented in Table 1. The highest levels of pyritic sulfur were found in shale samples S3 and S5. Trace elements in pyrite not detectable by XRD were determined by SEM. Small concentrations were found of Mn (0–0.69 wt%), Cu (0.06–0.37 wt%), Ni (0.01–0.22 wt%), Cd (0–0.19 wt%), Pb (0.03–0.12 wt%) and Co (0–0.01 wt%). Sphalerite was found only in one sample from the Kosov quarry (S5). Some sphalerite grains are enriched in Cd (up to 2.39 wt%).

3.3. Porous texture

Differences can be found in the terminology used by different authors, particularly in the use of the terms macroporosity, microporosity and nanoporosity. For sorption methods and for mercury porosimetry, pores are usually classified on the basis of their characteristic diameter, according to the IUPAC classification: <0.5 nm – ultra-microporosity, 0.5–2.0 nm – microporosity, 2.0–50 nm – mesoporosity, >50 nm – macroporosity [44]. Dubinin classified pores with radii from 1.5 nm to 100 nm as transient pores, and he classified pores with radii < 1.5 nm as micropores. In modern terminology these are also called nanopores [45]. When SEM is used, some authors distinguish only between small and large pores > 50 nm [46], while other authors report the pore sizes [47,48].

The results of the analysis of the shale porous system of samples S1–S7 are presented in Table 4. Helium density, specific surface area, parameters of microporous texture, parameters of meso- and macropore texture, and porosity, were determined. The specific surface S_{BET} is a standard parameter characterizing mainly the range of meso- and macropores. The applicability of the BET isotherm is limited to relative pressures 0.05–0.30, so it does not account for the presence of the smallest micropores and for capillary condensation. The S_{BET} surfaces of the shale samples ranged from a low value of 2.6–12.9 m^2.g^{-1}. The BET isotherms of the shale samples corresponded to type IV according to Brunauer's classification for a mesoporous adsorbent [44], and showed a hysteresis loop related to capillary condensation in mesopores. The hysteresis loops were of type H3 with parallel and almost horizontal adsorption and desorption branches of the isotherms (Fig. 7), which have been attributed to slit pores or to inner cavities of irregular shapes. The lowest extent of hysteresis, i.e., the lowest mesopore volume, was observed in sample S3, where the prevailing fraction of micropores was within the total pore volume

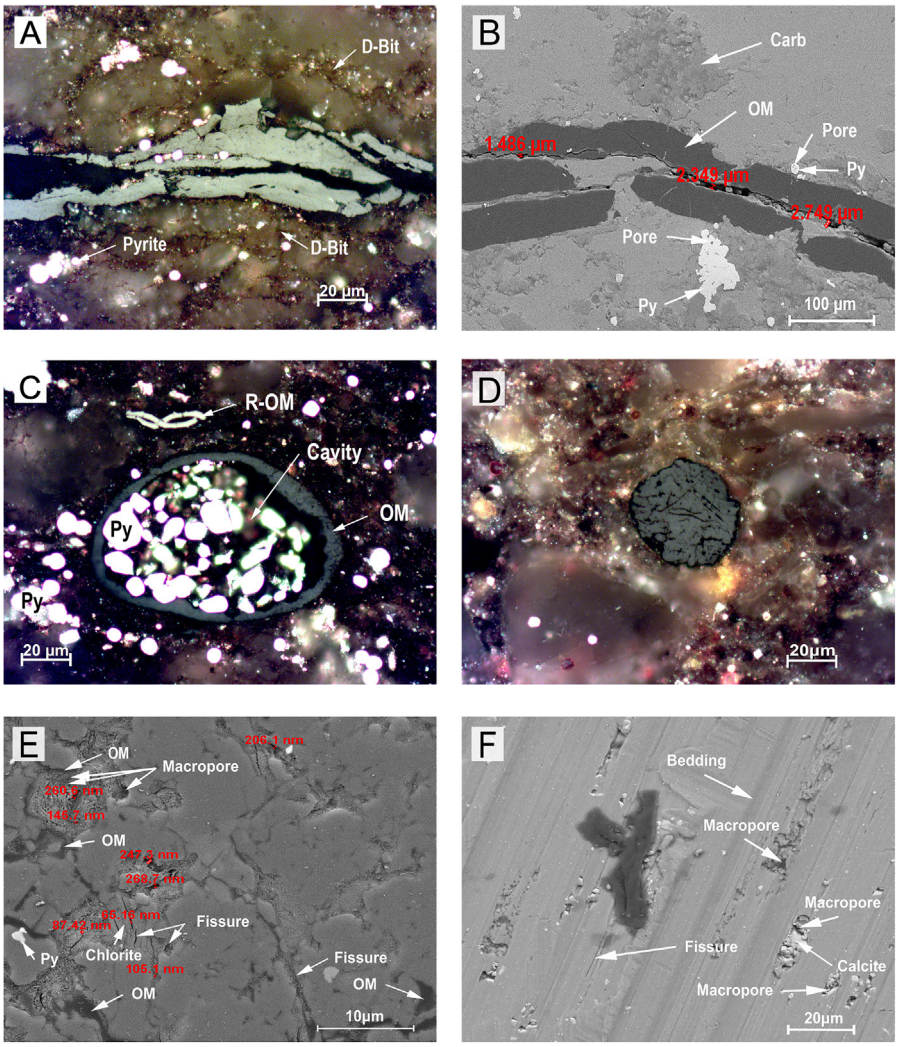

Fig. 6. A–F. Optical microscopy (A, C, D) and SEM (B, E, F) images of basic types or organic matter, pores and fissures in Silurian shales, Barrandian Basin: A – Graptolite fragments with fissures and pores in the mineral matrix with dispersed dark bitumen (D-Bit) and bright pyrite framboids and crystals (Pyrite) – sample 7. B – Fissures between the clay mineral matrix with carbonates (Carb) and the edge of the graptolite (OM), pores between pyrite crystals in clusters and in framboids – sample S7. C – Recycled, highly reflective graptolite (R-OM) with random reflectance R = 1.95% over the chitinozoan cut (R = 0.80%) with a cavity filled with crystalline pyrite - sample S3. D – A drop of non-granular bitumen (R = 0.87%) with surface inhomogenities in a clayey matrix with quartz grains – sample 2. E – Pores and fissures in clayey matrix and dark grey bitumen particles (OM) in mineral matter – sample S6. F – Dark fragment of zooclasts, macropores and fissures in a diagenetically arranged clay matrix with bedding lines and calcite admixtures – sample S-5.

Table 3
Mineral composition of shale samples.

Sample	Mineral (wt%)						
	Chlorite	Illite	Quartz	K-feldspars	Plagioclase	Calcite	Gypsum
S1	9	17	13	2	20	39	0
S2	8	19	15	0	21	37	0
S3	24	38	16	0	8	16	0
S4	5	23	30	0	21	21	0
S5	14	51	10	3	11	10	1
S6	38	28	16	0	18	0	0
S7	0	0	24	0	0	76	0

(V_{micro} + V_{mm}). This was also indicated by the most pronounced difference between porosity according to Hg porosimetry Por_{Hg} and according to calculated porosity Por_{calc}. The BET specific surface does not correlate with the porosity related to meso- and macropores.

From the low pressure isotherm of CO_2 sorption in Dubinin coordinates, low micropore volumes were identified, ranging from 0.0055 $cm^3.g^{-1}$ in sample S5 with the lowest total porosity, to 0.0137 $cm^3.g^{-1}$ in sample S4. Contrary to theoretical presumptions, based on the sorption mechanisms of N_2 and CO_2 sorption (see Section 2.2.5), the BET specific surface increases with increasing micropore volume (Fig. 8). The coefficient of determination R^2 = 0.838 indicates that for N_2 sorption only some the micropores are included in the S_{BET} surface. Ross and Bustin [10] reported the

Table 4
Characterization of the porous texture of the shale samples.

Sample	ρ_{He}	ρ_{Hg}	Por_{calc}	Por_{Hg}	S_{BET}	V_{micro}	r_{modus}	V_{mm}	V_{meso}	S_{mm}	r_{avr}
	($g.cm^{-3}$)		(%)		($m^2.g^{-1}$)	($cm^3.g^{-1}$)	(nm)	($cm^3.g^{-1}$)		($m^2.g^{-1}$)	(nm)
S1	2.6738	2.17	18.8	13.9	11.7	0.0097	0.67	0.0643	0.0106	2.9	303
S2	2.6845	2.32	13.6	10.5	10.6	0.0098	0.64	0.0454	0.0155	4.3	65
S3	2.6225	2.41	8.1	0.9	2.6	0.0057	0.66	0.0036	0.0014	0.5	4
S4	2.6561	2.33	12.3	10.5	12.9	0.0137	0.65	0.0451	0.0197	5.9	61
S5	2.6320	2.51	4.6	0.47	4.6	0.0055	0.66	0.0019	0.0008	0.3	4
S6	2.6263	2.46	6.3	4.8	10.3	0.0094	0.66	0.0196	0.0175	4.6	8
S7	2.7011	2.21	17.8	10.9	6.6	0.0061	0.65	0.0490	0.0244	5.4	27

ρ_{He} – helium density, ρ_{Hg} – bulk density, Por_{calc} – porosity ($(\rho_{He} - \rho_{Hg})/\rho_{He}).100$), Por_{Hg} – porosity according to Hg porosimetry, S_{BET} – specific surface area, V_{micro} – volume of micropores, r_{mode} – modus of micropores radii, V_{mm} – volume of meso- and macropores, V_{meso} – volume of mesopores, S_{mm} – surface area of meso- and macropores, r_{avr} – average pore radius.

same relation between S_{BET} and V_{micro}. The mode of pore diameters was within a narrow range between 0.64 and 0.66 nm (Fig. 9), which corresponds to characteristic energies E of shales with close values of the sorption potential [36].

A comparison of meso- and macropore volumes determined by the Hg intrusion method is presented together with the micropore volumes and the porosity for each shale sample in Table 4. With the exception of samples S3 and S5, the total meso- and macropore volumes are an order of magnitude higher than the micropore volumes. Samples S3 and S5 showed the highest fraction of micropores in the total pore volume (61.3% for S3 and 74.3% for S5), and at the same time the lowest fraction of meso- and macropores (Fig. 10B). The largest mesopore fraction (60.3%) was found in sample S6, and the largest macropore fraction (72.6%) was found in sample S1 (Fig. 10A).

3.4. Microstructure morphology

The pores in the shales examined here are of various types and sizes, including 1) pores in organic matter, 2) interparticle pores within detrital and authigenic grains of inorganic minerals, and 3) intraparticle pores between detrital grains and others related to authigenic crystals.

The pores of organic matter are isolated pores within organic matter that are produced by the maturation process. The rare pores in organic matter tend to be slightly irregular oval, round or polygonal in shape. Their sizes ranged from tens to hundreds of nanometers. It was found that graptolite (Figs. 6A and B) and chitinozoan (Fig. 6C) fragments without pores were common.

Interparticle pores occur especially between comparatively big irregular grains of calcite and plate aggregates of clay minerals predominantly illite (Fig. 6E). Most intragranular pores are located along the cleavage planes of clay matrix and chlorite (Fig. 6E), and within pyrite framboids (Fig. 6B) and calcite crystals. These pores show little preferential orientation.

Another significant feature of the shales investigated here is well-expressed schistosity, which is sometimes partly emphasized by the presence of fractures (Fig. 6F). Most of the fractures were found in more mature shale sample S6 (Fig. 6E). The fractures between grains of minerals range from tens of nm frequently up to 300 nm in width, and are between 2 and 12 μm in length. The fractures developed at the edge of the organic matter and also in organic particles, mainly in graptolites (Fig. 6D). Partial dissolution of some detrital calcite resulted in the formation of intraparticulate pores (Fig. 6F).

Marked differences in sediment diagenesis were observed by SEM and documented by representative figures Fig. 6E and F. A lower degree of diagenetic alteration was found in sample S3 and S5 with preferred bedding (Fig. 6F). An advanced degree of diagenesis was observed in other samples S1, S2, S7, and namely S6. The high reflectance value in graptolites in S6 was due to the hidden thermal effect of a volcanic body. However, no diagenetic pressure effects were apparent.

The occurrence of pyrite in vein-like and vein accumulations, together with rare occurrences of sphalerite in the mature samples (S5, S6), and higher concentrations of chlorite, provided evidence that some accumulations of schists were affected by postdiagenetic alterations.

4. Discussion

4.1. Effect of thermal maturity and shale components on sorption capacity

The organic materials encountered in Barrandian Silurian shales include mainly graptolite and chitinozoan particles, with rounded particles and disseminated fragments of bitumen, and minor highly reflecting particles of redeposited organic matter and fine-grained detritus particles. This uniform assemblage of organic particles identified and measured in Barrandian shales is comparable to those of other Lower Paleozoic sediments [49], particularly from Scandinavia [29], Canada [50–52], selected samples of shales in Europe [11] and China [53,54]. Due to the absence of vitrinite in Lower Paleozoic sediments up to Devonian/Carboniferous age, the degree of maturation is expressed by bitumen reflectance [54] and by graptolite and chitinozoan reflectance [55,56]. The average reflectance value of bitumen and graptolites is often converted mathematically to the equivalent vitrinite reflectance by the equations summarized Suchý et al. [56], Feng and Chen [57]. In the part of the Barrandian Basin studied here, the graptolite reflectance values range from 0.56% to 1.09%, and to 1.76% in sample S6.

The lowest reflectance value was measured in sample S4, with dominant quartz. This extreme is probably caused by origin of S4 from upper Silurian Kopanina Formation (Table 1 and Fig. 2) and intense silicification, which suppressed the influence of maturation of organic matter, particularly graptolites. The highest reflectance value measured for sample S6 is probably related to rapid heating of the organic matter (particularly graptolite periderm) due to an igneous intrusion nearby [43]. The reflectance values of the samples, with the exception of sample S4, correspond to the hydrocarbon generation stage, ranging from the oil window to the wet-gas condensate zone [58].

According to several authors [2–4,9,10,14,16,23], the adsorption capacity for CH_4 is affected mainly by thermal maturation, TOC, and mineral matter. Although Ross and Bustin assume that thermal maturation has a positive effect on the sorption capacity of shales [10], in the case of the samples studied here, no direct correlation was observed between thermal maturation and TOC normalized excess sorption capacity or normalized Langmuir sorption capacity

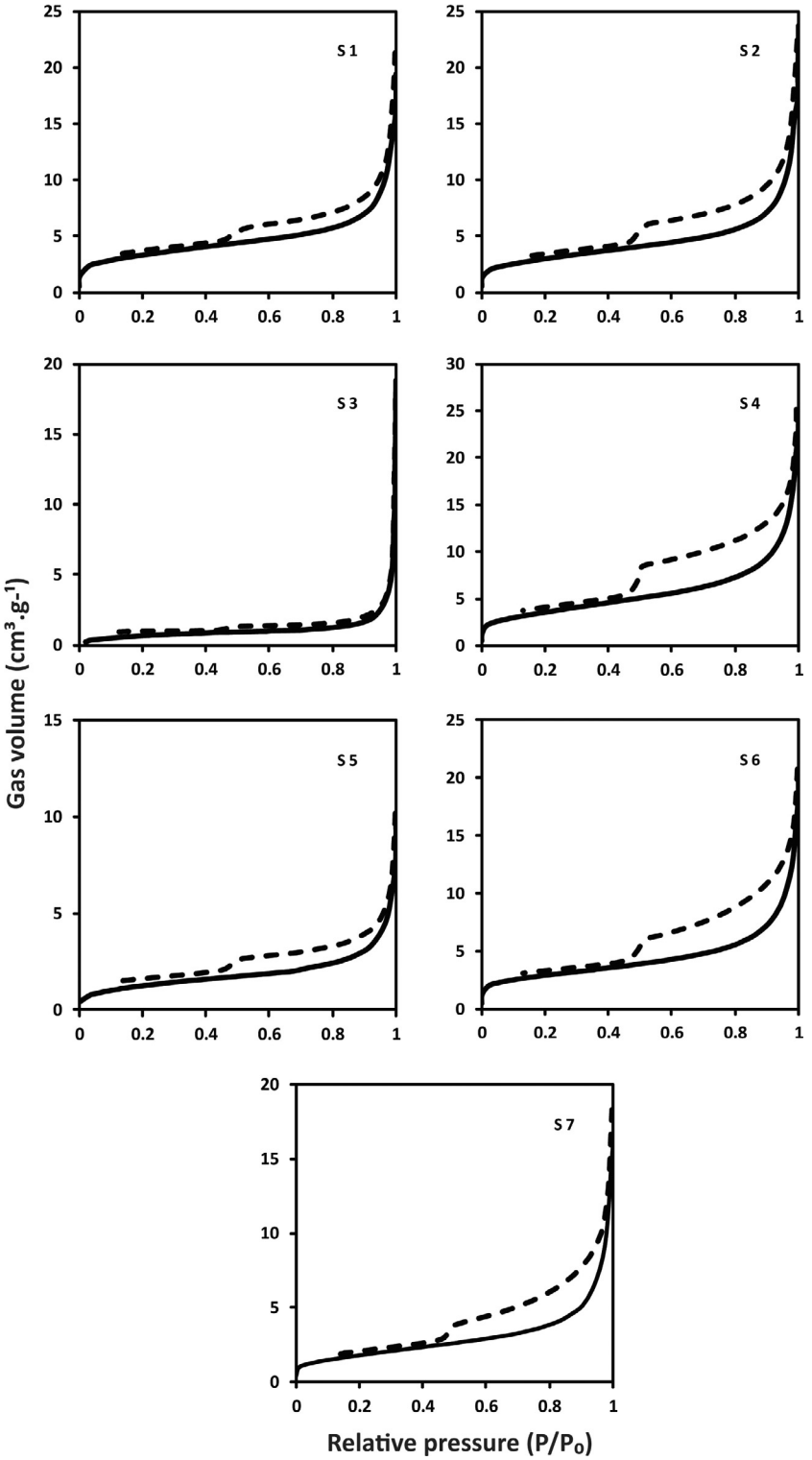

Fig. 7. Hysteresis loops of N_2 isotherms on shale samples S1–S7 (solid line – adsorption isotherm, dashed line – desorption isotherm).

(Fig. 11). Sample S6 had the highest R_r value and a very low normalized sorption capacity. In addition, no relation between thermal maturation and TOC content was observed in the shale samples, possibly due to low reflectance values R_r, low TOC contents, the general character of the mineral phase, and other factors associated with the regional distribution and the conditions in the depositional environment.

The CH_4 maximum excess sorption capacity n_{max} and the Langmuir sorption capacity n_L were positively correlated with TOC (see the graph in Fig. 12). The highest sorption capacities were found in samples S3 (0.088 mmol.g^{-1}) and S5 (0.075 mmol.g^{-1}), with the highest TOC values of 2.37 and 2.33 wt%. Similar correlations between sorption capacity and TOC have been found in samples from various parts of the world [2,11]. Wang et al. reported a broad

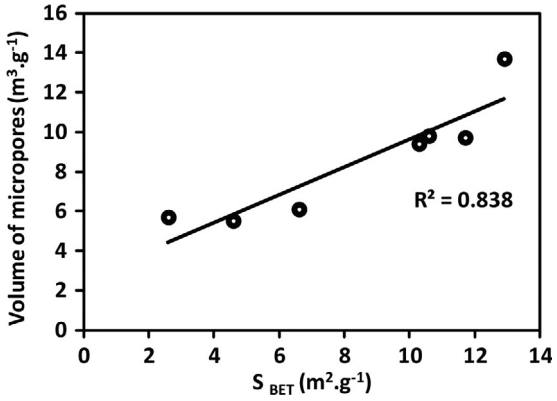

Fig. 8. Correlation between micropore volume (V_{micro}) and BET surface area (S_{BET}).

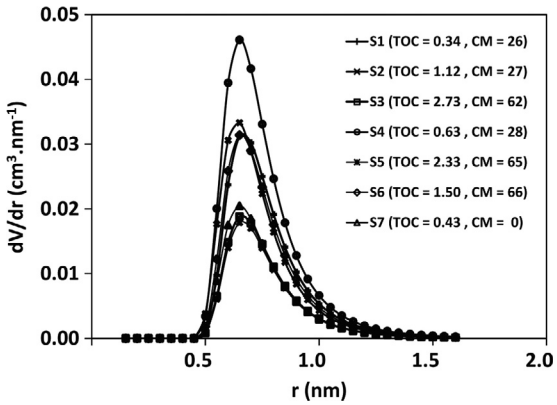

Fig. 9. Micropore size distribution interpreted by CO_2 adsorption data, (TOC (wt%) – total organic carbon, CM (wt%) – clay minerals).

linear dependence between TOC and CH_4 sorption capacity in Sichuan Shales of China [16], where the organic matter is a primary factor controlling CH_4 sorption in Paleozoic shales (Cambrian and Silurian). A similar dependence is found for North American shales. Wang et al. also found that the CH_4 sorption capacity tends to decrease with the age of the sediment. This is corroborated by the CH_4 sorption capacities of Permian shales, which were higher than the sorption capacities of Silurian and Cambrian shales, that are characteriezed by a lower TOC. The following conclusions can be drawn for the shale samples studied here, on the basis of the facts presented above, and in agreement with published data:

a) thermal maturation is not the only factor controlling the sorption capacity, but is only a contributing factor. Most samples have an R_r value close to 1%, but there are exceptions. Sample S4 has an extremely low R_r value of 0.56%, and sample S6 has a high R_r value of 1.76% [14,59];
b) the positive relation between TOC and methane sorption capacity shows that the content of organic matter is a key factor determining the sorption capacity of shales [11]. Lower values of the coefficient of determination for this relation (R^2 = 0.8339 for n_{max} and R^2 = 0.8037 for n_L, see Fig. 12) and the exponential decrease in the TOC normalized values n_{max} and n_L as a function of TOC (Fig. 12) show that the sorption capacity is affected by additional factors, e.g. the content of clay minerals.

Conclusion b) should not be generalized. For example, Gasparik et al. presented the results of one Paleozoic shale and five Mesozoic shales from Netherlands, in which the sorption capacities did not

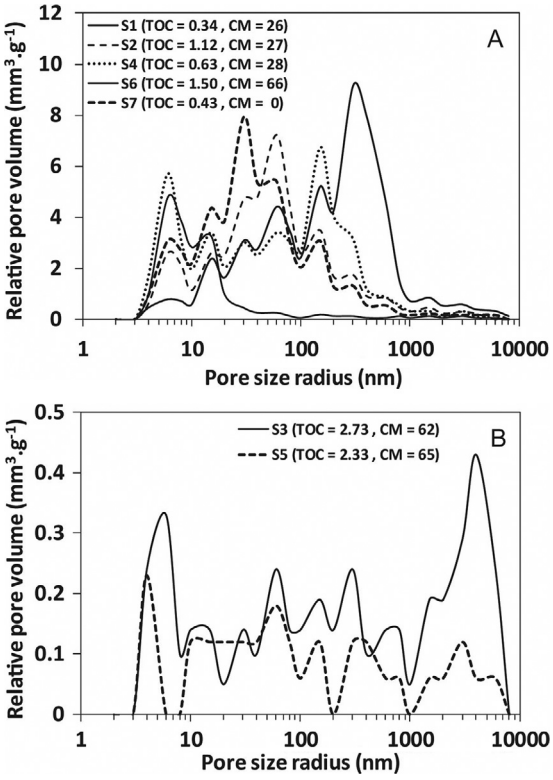

Fig. 10. Distribution of meso- and macropores according to Hg porosimetry: A) samples S1, S2, S4, S6 and S7, B) samples S3 and S5, (TOC (wt%) – total organic carbon, CM (wt%) – clay minerals).

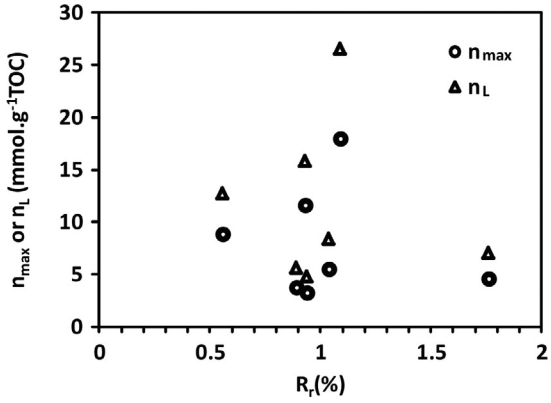

Fig. 11. Effect of thermal maturity on the TOC-normalized maximum measured excess sorption (n_{max}) and the Langmuir sorption capacity (n_L).

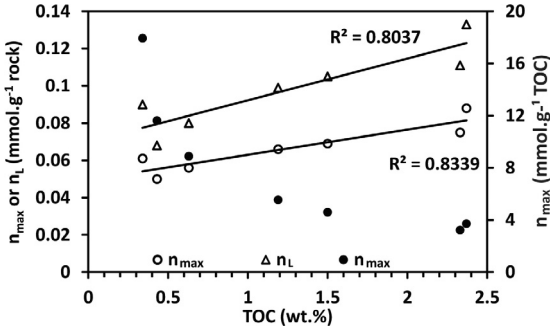

Fig. 12. Maximum measured excess sorption (n_{max}) and Langmuir sorption capacity (n_L) on rock, or TOC normalized (full symbol) as a function of TOC.

follow the TOC dependence [3]. This can been explained by the great variability in the chemical and physical properties of shales of different geological age and of different provenance.

A positive effect of clay minerals on sorption capacity has been confirmed for our shale samples (Fig. 13). This indicates that their sorption capacity is not controlled only by TOC. The same conclusion was drawn by Gasparik et al. for Dutch shales [3], but has not been confirmed for shales from Northern Europe [11]. Tan et al. failed to observe a similar relation either in Chinese shales or in North Australian shales [2]. Yang et al. derived a linear combination approach for predicting the Langmuir sorption capacities of individual shale components (mineral and organic matter), and found that clay minerals contributed 28.6% to the total sorption capacity and that organic matter contributed 67.6% [21]. Merkel et al. concluded that the sorption capacities of pure clay minerals are about 10 times lower than the sorption capacities of anthracite (approximately 1.2 mmol.g^{-1}), used as a model substance for the organic matter. They can therefore contribute significantly to the sorption capacity only in shales with low TOC [17]. The sorption capacity of Silurian shales from the Barrandian Basin is on an average only one twentieth of the anthracite sorption capacity and the sorption capacity of illite and chlorite [12] is more or less comparable to the total sorption capacities of the shales studied here. It can be assumed that the observed effect of clay minerals is due to low TOC levels in our shale samples.

For a study of the effect of clay minerals on methane sorption capacity, it is important to take into account not only their total content but also their composition, which reflects the diagenetic evolution and depositional environments. For example, montmorillonite is eventually transformed into illite during diagenesis, and this will affect the sorption capacity of shales. In the shale samples studied here, we observed a possible relation between methane sorption capacity and illite content (with an R^2 value of 0.6474), and chlorite content (with an R^2 value of 0.4117), see Fig. 13. However, Wang et al. found no relationship between the methane sorption capacity of shales and the content of illite or montmorillonite [16].

4.2. The effect of porous texture on sorption capacity

A microscopic study of various pores and dominant fissures in organic and inorganic matter was carried out by the use of conventional scanning electron microscopy with GAD detector. Pore structure characteristics of shales of various age and provenience have been investigated recently with the use of field emission scanning electron microscopy [e.g., 54,60–62]. Three pore groups were found in the shales examined here. It has been found that most

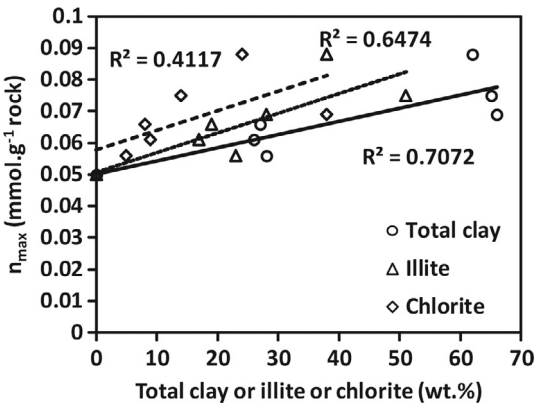

Fig. 13. Maximum measured excess sorption (n_{max}) as a function of i) total content of clays, ii) content of illite and iii) content of chlorite.

of the carbonaceous fragments of graptolites and bitumens in the Silurian shales from the Barrandian Basin contain small organic pores. They are often smaller in size (tens to hundreds of nm). The absence or the presence of pores in carbonaceous particles at a similar degree of maturity depends on the composition and the type of individual carbonaceous particles [59]. Not all organic matter appears to develop pores in sediments of different ages [60,61]. Microscopic observation indicated that changes in the volume, morphology and distribution of organic pores are not systematically dependent on the progress of thermal maturation. According to their random reflectance range of 0.56–1.09%, the samples belong to the discussed region of the formation and development of pores in the organic matter. Tang et al. [63] observed numerous pores in the organic matrix of a shale from the Ordos Basin (China) even at reflectance of R_r = 0.72%. Curtis et al. [59] found organic pores in Woodford Shale even at reflectance of R_r = 1.23–1.67%, while no organic pores were observed in organic matrix with reflectance of R_r < 0.90%.

Micrographs (Fig. 6) show that there are many more pores and cracks in the mineral phase, particularly in clay minerals. Interparticle pores are the most significant pore group in shales worldwide, and often predominate over intraparticle pores in inorganic matter [54,60,62,64]. Nanopores were found especially between individual grains in framboidal pyrite. Intraparticle pores are present within some bigger quartz and calcite grains. Partial dissolution of bigger detrital calcite grains results in the formation of intraparticle pores. Similar dissolution-related micropores to macropores were found by Fishman et al. [60] in the Upper Jurassic clay formation in the North Sea, and by Yang et al. [54] in Lower Silurian shales, China. For the Silurian black shales, however, there is a highly significant occurrence of variable fractures, especially fractures that run parallel with the original sedimentary bending.

The porous system can be quantitatively characterized using sorption methods (CO_2, N_2) and mercury porosimetry, both of which are widely utilized for this purpose [2,9,10,22,46].

Micropores are the most important part of the porous system for the sorption capacity of shale, due to the high adsorption potential of these very narrow pores with radii < 2 nm. Organic matter is considered to be a major bearer of the shale microporous texture, though clay minerals can also make a significant contribution to the total micropore volume [2]. The microporosity is attributed to an interlayer span of smectite minerals, while aggregates of clay mineral particles contain mesopores between the individual particles. Some authors have stated that clay minerals are mostly meso- and macroporous [15,58,59]. However, Ross and Bustin determined micropore volumes of major clay minerals using low pressure CO_2 sorption, and they present V_{micro} = 0.008 cm^3.g^{-1} for illite and V_{micro} = 0.0013 cm^3.g^{-1} for chlorite [10]. These values are within the order of micropore volumes determined for shales in our study.

A positive correlation was found between TOC and the maximum measured sorption capacity (see Fig. 12), and organic matter is considered to be a key factor controlling the sorption capacity of shale. However, for the samples studied here, the precondition of a positive correlation between micropore volume V_{micro} and TOC, according to findings of Ross and Bustin [10] and Chalmers and Bustin [14] has not been met. Nevertheless, there was a strong positive correlation between the micropore percentage and TOC (R^2 = 0.8754) (Fig. 14). The correlation between TOC and total porosity (Por_{calc}) was negative, and the shale samples with the highest TOC and the highest micropore percentage (61.3% in S3, 74.3% in S5) had the lowest porosity, due to the small volumes of mesopores and macropores (Fig. 15). Most of the meso- and macropores were present in the inorganic component of the shale samples. The percentage of mesopores and macropores is up to eight times higher than the percentage of micropores (meso- and

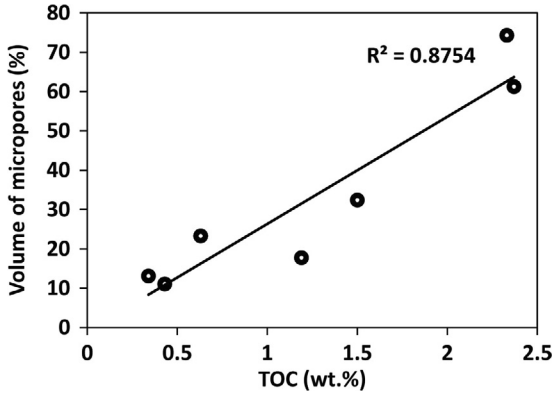

Fig. 14. The relationship between TOC content and the percentage of micropores ($\%V_{micro}$).

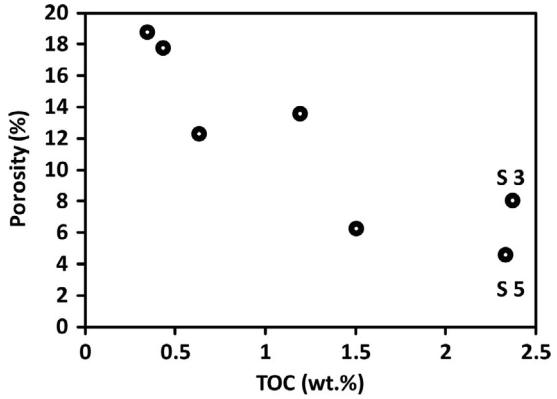

Fig. 15. The relationship between TOC content and porosity (Por_{calc}).

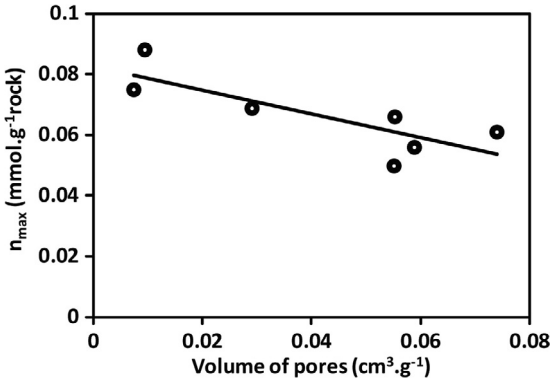

Fig. 17. Maximum measured excess sorption (n_{max}) as a function of the total volume of pores.

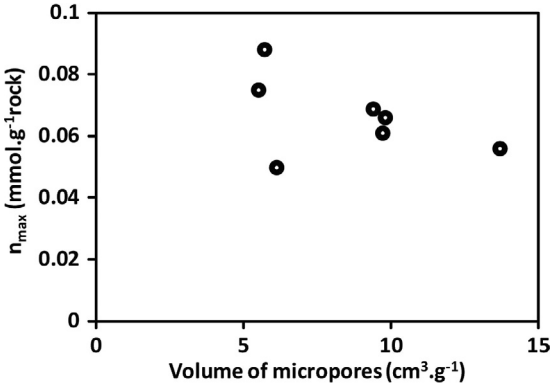

Fig. 18. Maximum measured excess sorption (n_{max}) as a function of the volume of micropores (V_{micro}).

macropores: S1 86.9%, S7 88.9%), with the exception of samples S3 and S5. By contrast, Yang et al. observed a positive correlation between TOC and porosity in Silurian shales from the southern Sichuan Basin, China. The correlation increased with increasing degree of maturity up to bitumen reflectance R_{ekv} of 2.5%, and then decreased with increasing degree of maturity [54]. Taking into account a small quantity of micropores (see Table 4), the total porosity of the shale samples is a function of the meso- and macropores, as is evident from the dependence $V_{mm} \times Por_{calc}$ (Fig. 16).

A decrease in maximum sorption capacity (n_{max}) as a function of total pore volume was observed (Fig. 17) when the highest sorption capacities were found in the shale samples with the highest percentage of micropores (S3, S5), while the lowest sorption capacity was found in the sample with the highest percentage of macropores (S1). The assumption that the sorption capacity is a function mainly of the microporous system of shales contradicted the observed negative dependence of the methane maximum sorption capacity (n_{max}) on the absolute micropore volume (Fig. 18). However, there was an unambiguous positive relation between the methane maximum sorption capacity n_{max} and the percentage of micropores (Fig. 19).

The results for high pressure sorption, which represent the total sorbed gas content (Table 2), do not enable a distinction to be

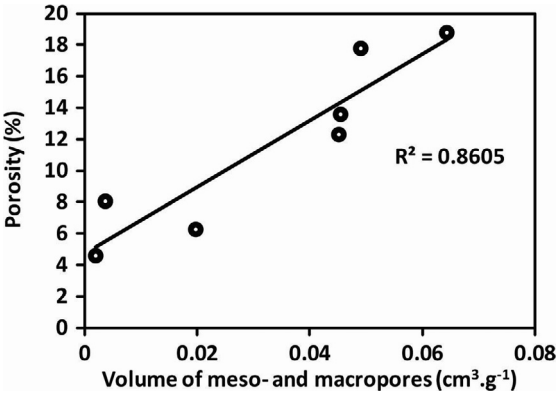

Fig. 16. The relationship between volume of meso- and macropores (V_{mm}) and porosity (Por_{calc}).

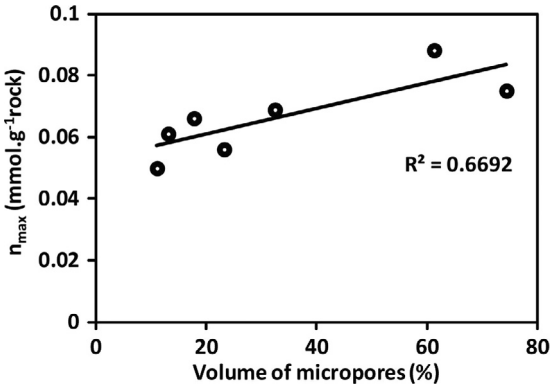

Fig. 19. Maximum measured excess sorption (n_{max}) as a function of the percentage of micropores ($\%V_{micro}$).

made between the amount of gas filling the volume of the micropores and the amount of gas sorbed on the surface of the meso- and macropores.

5. Conclusions

High-pressure methane sorption isotherms were measured on seven Silurian shales from Barrandian Basin, Czech Republic. The effects of organic maturity, TOC contents, inorganic components, and pore size distribution on the sorption capacity have been investigated. The following conclusions can be drawn:

1. The thermal maturity, characterized by random reflectance of graptolite values close to 1% for most of the samples, had no effect on the TOC normalized sorption capacity. Microscopic observations showed that changes in volume, morphology and distribution of organic pores are also not systematically dependent on an increasing degree of thermal maturity.
2. A positive correlation between TOC in the range 0.34–2.73 wt% and methane excess sorption capacity in the range 0.050–0.088 mmol.g^{-1} identifies the content of organic matter as a factor controlling a significant part of the sorption capacity of shale. The sorption capacity of the shale samples was positively affected by clay minerals (from 0 to 66 wt%), due to the relatively low TOC content.
3. No correlation of the sorption capacity with micropore volume was found.
4. The total porosity of the shale samples ranged from 4.6 to 18.8%. Higher porosity values are mainly contributed by meso- and macropores, since micropores are several times less abundant. Samples with these parameters had lower sorption capacities than samples with low porosity, low abundance of meso- and macropores, and prevailing micropore abundance. Although the samples with the highest micropore abundance had the lowest absolute micropore volume values, they had the highest sorption capacity and also the highest content of bitumen forms, the highest TOC content and the highest clay minerals content.

Acknowledgements

This work was carried out in the framework of the Centre for Texture Analysis project within the Prague Competitiveness Operational Program, (No.: CZ.2.16/3.1.00/21538). The authors thank Robin Healey for correcting the language of the submitted manuscript and also of the revised manuscript.

References

[1] Gasparik M, Gensterblum Y, Ghanizadeh A, Weniger P, Krooss BM. High-pressure/high-temperature methane-sorption measurements on carbonaceous shales by the manometric method: experimental and data-evaluation considerations for improved accuracy. SPE J 2015;174543:20.
[2] Tan J, Weniger P, Krooss BM, Merkel A, Horsfield B, Zhang J, et al. Shale gas potential of the major marine shale formations in the Upper Yangtze Platform, South China, Part II: methane sorption capacity. Fuel 2014;129:204–18.
[3] Gasparik M, Ghanizadeh A, Bertier P, Gensterblum Y, Bouw S, Krooss BM. High-pressure methane sorption isotherms of black shales from The Netherlands. Energy Fuels 2012;26:4995–5004.
[4] Zhang T, Ellis GS, Ruppel SC, Milliken K, Yang R. Effect of organic-matter type and thermal maturity on methane adsorption in shale-gas systems. Org Geochem 2012;47:120–31.
[5] Weishauptová Z, Medek J, Kovář L. Bond forms of methane in porous system of coal II. Fuel 2004;83:1759–64.
[6] Curtis JB. Fractured shale gas systems. AAPG Bull 2002;86:1921–38.
[7] Aringhieri R. Nanoporosity characteristics of some natural clay minerals and soils. Clays Clay Miner 2004;52:700–4.
[8] Cheng AL, Huang WL. Selective adsorption of hydrocarbon gases on clays and organic matter. Org Geochem 2004;35:413–23.
[9] Hou Y, He S, Yi J, Zhang B, Chen X, Wang Y, et al. Effect of pore structure on methane sorption potential of shales. Pet Explor Dev 2014;41(2):272–81.
[10] Ross DJK, Bustin RM. The importance of shale composition and pore structure upon gas storage potential of shale gas reservoir. Mar Pet Geol 2009;26:916–27.
[11] Gasparik M, Bertier P, Gensterblum Y, Ghanizadeh A, Krooss BM, Littke R. Geological controls on the methane storage capacity in organic-rich shales. Int J Coal Geol 2014;123:34–51.
[12] Ji L, Zhang T, Milliken K, Qu J, Zhang X. Experimental investigation of main controls to methane adsorption in clay-rich rocks. Appl Geochem 2012;27:2533–45.
[13] Dubinin M. Physical adsorption of gases and vapors in micropores. Prog Surf Membr Sci 1975;9:1–70.
[14] Chalmers GRL, Bustin RM. The organic matter distribution and methane capacity of the Lower Cretaceous strata of Northeastern British Columbia, Canada. Int J Coal Geol 2007;70:223–39.
[15] Chalmers GRL, Bustin RM. Lower Cretaceous gas shales in northeastern British Columbia, Part I: geological controls on methane sorption capacity. Bull Can Pet Geol 2008;56:1–21.
[16] Wang S, Song Y, Cao T, Song X. The methane sorption capacity of Paleozoic shales from the Sichuan Basin, China. Mar Pet Geol 2013;44:112–9.
[17] Merkel A, Fink R, Littke R. The role of pre-adsorbed water on methane sorption capacity of Bossier and Haynesville shales. Int J Coal Geol 2015;147–148:1–8.
[18] Yuan W, Pan Z, Li X, Yang Y, Zhao C, Connell LD, et al. Experimental study and modelling of methane adsorption and diffusion in shale. Fuel 2014;117:509–19.
[19] Yang F, Ning Z, Zhang R, Zhao H, Krooss BM. Investigations on the methane sorption capacity of marine shales from Sichuan Basin, China. Int J Coal Geol 2015;146:104–17.
[20] Wang G, Ju Y, Yan Z, Li Q. Pore structure characteristics of coal-bearing shale using fluid invasion methods: a case study in the Huainan-Huaibei Coalfield in China. Mar Pet Geol 2015;62:1–13.
[21] Reexer TFT, Benham MJ, Aplin AC, Thomas KM. Methane adsorption on shale under simulated geological temperature and pressure conditions. Energy Fuels 2013;27:3099–109.
[22] Khosrokhavar R, Wolf KH, Bruining H. Sorption of CH_4 and CO_2 on a carboniferous shale from Belgium using a manometric setup. Int J Coal Geol 2014;128–9:153–61.
[23] Rexer TFT, Mathia EJ, Aplin AC, Thomas KM. High-pressure methane adsorption and characterization of pores in Posidonia shales and isolated kerogens. Energy Fuels 2014;28:2886–901.
[24] Kříž J. In: Chlupáč I, Havlíček V, Kříž J, Kukal Z, Štorch P, editors. Palaeozoic of the Barrandian (Cambrian to Devonian). Prague: Czech Geological Survey; 1998. p. 79–101.
[25] Kříž J, Degardin JM, Ferretti A, Hansch W, Guttiérez Marco JC, Paris F, et al. Silurian stratigraphy and palaeogeography of Gondwanan and Perunican Europe. In: Landing E, Johnson ME, editors. Silurian land and seas. Paleogeography outside Laurentia, 493. New York State Museum Bulletin; 2003. p. 105–78.
[26] Goodarzi F. Organic petrography of graptolite fragments from Turkey. Mar Pet Geol 1984;10:215–30.
[27] Suchý V, Sýkorová I, Stejskal M, Šafanda J, Machovič V, Novotná M. Dispersed organic matter from Silurian shales of the Barrandian Basin, Czech Republic: optical properties, chemical composition and thermal maturity. Int J Coal Geol 2002;53:1–25.
[28] Suárez-Ruiz I, Flores D, Filho JGM, Hackley P. Review and update of the applications of organic petrology: Part 1. Geological applications. Int J Coal Geol 2012;99:54–112.
[29] Petersen HI, Schovsbo NH, Nielsen AT. Reflectance measurements of zooclasts and solid bitumen in Lower Paleozoic shales, southern Scandinavia: correlation to vitrinite reflectance. Int J Coal Geol 2013;114:1–18.
[30] Haeri-Ardakani O, Sanei H, Lavoie D, Chen Z, Jiang Ch. Geochemical and petrographic characterization of the Upper Ordovician Utica Shale, southern Quebec, Canada. Int J Coal Geol 2015;138:83–94.
[31] ISO 7404-3. Methods for the petrographic analysis of coal - Part 3: method of determining Maceral group composition. Geneva, Switzerland: International Organization for Standardization; 2009. p. 14.
[32] Pouchou JL, Pichoir F. "PAP" (φ-ρ-Z) procedure for improved quantitative microanalysis. In: Armstrong JT, editor. Microbeam analysis. San Francisco: San Francisco Press; 1985. p. 104–6.
[33] Washburn EW. The dynamics of capillary flow. Phys Rev 1921;17:273–83.
[34] Brunauer S, Emmett PH, Teller E. Adsorption of gases in multimolecular layers. J Am Chem Soc 1938;60:309–24.
[35] Dubinin MM. Adsorption in micropores. J Colloid Interface Sci 1967;23:487.
[36] Medek J. Possibility of micropore analysis of coal and coke from the carbon dioxide isotherm. Fuel 1977;56:131–3.
[37] Weishauptová Z, Přibyl O, Sýkorová I, Machovič V. Effect of bituminous coal properties on high pressure sorption. Fuel 2015;139:115–24.
[38] Gensterblum Y, van Hemert P, Billemont P, Busch A, Charriére D, Li D, et al. European inter-laboratory comparison of high pressure CO_2 sorption isotherm. I: activated carbon. Carbon 2009;47:2958–69.
[39] Sakurovs R, Day S, Weir S, Duffy G. Temperature dependence of sorption of gases by coal and charcoals. Int J Coal Geol 2008;73:250–8.

[40] Setzmann U, Wagner W. A new equation of state and tables of thermodynamic properties for methane covering the range from the melting line to 625 K at pressures up to 1000 MPa. J Phys Chem Ref Data 1991;20:1061–155.
[41] Cole GA. Graptolite-Chitinozoan reflectance and its relationship to other geochemical maturity indicators in the Silurian Quasaiba Shale, Saudi Arabia. Energy Fuels 1994;8:1443–59.
[42] Gentzis T, deFreitasd T, Goodarzi F, Melchin M, Lenz A. Thermal maturity of Lower Paleozoic successions in Arctic Canada. Am Assoc Pet Geol Bull 1996;80:1065–84.
[43] Suchý V, Dobeš P, Filip J, Stejskal M, Zeman A. Conditions for veining in the Barrandian Basin (Lower Palaeozoic), Czech Republic: evidence from fluid inclusion and apatite fission track analysis. Tectonophysics 2002;348:25–50.
[44] . London, U.K.: Butterworth; 1972.
[45] Dubinin MM. The potential theory of adsorption of gases and vapours for adsorbents with energetically nonuniform surfaces. Chem Rev 1960;60:235–41.
[46] Li Jij, Yin J, Zhang Y, Lu S, Wang W, Li Jin, et al. A comparison of experimental methods for describing shale pore features—a case study in the Bohai Bay Basin of eastern China. Int J Coal Geol 2015;152:39–49.
[47] Wang R, Gu Y, Ding W, Gong D, Yin S, Wang X, et al. Characteristics and dominant controlling factors of organic-rich marine shales with high thermal maturity: a case study of the Lower Cambrian Niutitang Formation in the Cen'gong block, southern China. J Nat Gas Sci Eng 2016;33:81–96.
[48] Guo X, Li Y, Liu R, Wang Q. Characteristics and controlling factors of micropore structures of the Longmaxi Shale in the Jiaoshiba area, Sichuan Basin. Nat Gas Ind 2014;B1:165–71.
[49] Goodarzi F. Dispersion of optical properties of graptolite epiderms with increased maturity in early paleozoic organic sediments. Fuel 1985;64:1735–40.
[50] Goodarzi F, Norford BS. Graptolites as indicators of the temperature histories of rocks. J Geol Soc London 1985;142:1089–99.
[51] Bertrand R, Héroux Y. Chitinozoan, graptolite, and scolecodont reflectance as an alternative to vitrinite and pyrobitumen reflectance in Ordovician and Silurian Strata, Anticosti Island, Quebec, Canada. Am Assoc Pet Geol Bull 1987;71:951–7.
[52] Riediger C, Goodarzi F, Macqueen RW. Graptolites as indicators of regional maturity in Lower Paleozoic sediments, Selwyn Basin, Yukon and Northwest territories, Canada. Can J Earth Sci 1989;26:2003–15.
[53] Wang X, Hoffknecht A, Jianxin X, Li Z, Chen S, Brocke R, et al. Thermal maturity of the Sinian and early Paleozoic in West Hubei, China, assessed by CAI, reflectance and geochemical studies. Stratigr Paleontol China 1987;2:19–45.
[54] Yang F, Ning Z, Wang Q, Zhang R, Krooss BM. Pore structure characteristics of lower Silurian shales in the southern Sichuan Basin, China: insight to pore development and gas storage mechanism. Int J Coal Geol 2016;156:12–24.
[55] Tricker PM. Chitinozoan reflectance in the Lower Palaeozoic of the Welsh Basin. Terra Nova 1992;4:231–7.
[56] Suchý V, Sandler A, Slobodník M, Sýkorová I, Flip J. Diagenesis to very low-grade metamorphism in lower Palaeozoic sediments: a case study from borehole Tobolka 1, the Barrandian Basin, Czech Republic. Int J Coal Geol 2015;140:41–62.
[57] Feng GX, Chen SJ. Relationship between the reflectance of bitumen and vitrinite in rocks. Nat Gas Ind 1988;8:20–4.
[58] Chalmers GRL, Ross DJK, Bustin RM. Geological controls on matrix permeability of Devonian Gas Shales in the Horn River and Liard basins, northeastern British Columbia, Canada. Int J Coal Geol 2012;103:120–31.
[59] Curtis ME, Sondergeld CH, Ambrose RJ, Rai ChS. Structural characterization of gas shales on the micro- and nano-scales. In: Canadian unconventional resources & international petroleum conference, (SPE-137693-MS). Alberta, Canada: Calgary; 19–21 October; 2010
[60] Fishman NS, Hackley PC, Lowers HA, Hill RJ, Egenhoff SO, Eberl DD, et al. The nature of porosity in organic-rich mudstones of the Upper Jurassic Kimmeridge Clay Formation, North Sea, offshore United Kingdom. Int J Coal Geol 2012;103:32–50.
[61] Zhao X, Li Q, Jiang Z, Zhang R, Li H. Organic geochemistry and reservoir characterization of the organic matter-rich calcilutite in the Sulu Sag, Bohai Bay basin North China. Mar Pet Geol 2014;51:239–55.
[62] Zhang Q, Liu R, Pang Z, Lin W, Bai W, Wang H. Characterization of microscopic pore structures in Lower Silurian black shale (S_1l), Southern Chongqing, China. Mar Pet Geol 2016;71:250–9.
[63] Curtis ME, Cardott BJ, Sondergeld CH, Rai ChS. Development of organic porosity in the Woodford Shale with increasing thermal maturity. Int J Coal Geol 2012;103:26–31.
[64] Loucks RG, Reed RM, Ruppel SC, Jarvie DM. Morphology, genesis, and distribution of nanometer-scale pores in siliceous mudstones of the Mississippian Barnet Shale. J Sediment Res 2009;79:848–61.